Temperature-independent field-induced charge separation at doped organic/organic interfaces: Experimental modeling of electrical properties

Michael Kröger,[1,*] Sami Hamwi,[1] Jens Meyer,[1] Thomas Dobbertin,[2] Thomas Riedl,[1] Wolfgang Kowalsky,[1] and Hans-Hermann Johannes[2,†]

[1]*Institut für Hochfrequenztechnik, Technische Universität Braunschweig, Schleinitzstrasse 22, 38106 Braunschweig, Germany*

[2]*Osram Opto Semiconductors GmbH, Leibnizstrasse 4, 93055 Regensburg, Germany*

(Received 16 February 2007; published 19 June 2007)

We examine field-induced charge-carrier separation at doped organic/organic heterointerfaces consisting of tetrafluorotetracyanoquinodimethane doped 4,4′,4″-tris(*N*-1-naphtyl-*N*-phenylamino)-triphenylamine as hole-transporting layer and Li-doped 1,3,5-tri(phenyl-2-benzimidazole)-benzene as electron-transporting layer. Low-temperature *I-V* characteristics, thickness-dependent *I-V* characteristics, and Kelvin probe measurements are used to model the energy-level alignment at the interface. No explicit temperature dependence is observed. Thickness-dependent *I-V* characteristics and Kelvin probe measurements give evidence for a 5-nm-thin depletion layer adjacent to the interface. Consistent with our experimental results, we propose a model of electrons tunneling through the depletion zone from the highest occupied molecular orbit of the hole-transporting material to the lowest unoccupied molecular orbit of the electron-transporting material. This generates an electron-hole pair, which dissociates under the intense electric field close to the interface.

DOI: 10.1103/PhysRevB.75.235321 PACS number(s): 73.61.Ph, 72.20.Jv, 81.05.Lg, 85.60.Jb

I. INTRODUCTION

Recently, charge-carrier separation at organic/inorganic or organic/organic interfaces within stacked organic light-emitting diodes (OLEDs) has been observed and has aroused a lot of interest because of its potential to dramatically enhance the quantum efficiency of OLEDs. Within stacked OLEDs, two or more emission layers are connected by introducing thin metal interlayers[1] or by employing so-called charge generation layers (CGLs).[2–10] Several different CGL architectures have been proposed, but in all cases they consisted either of doped organic/inorganic layer sequences[2–8] or doped organic/organic *p-n* junctions.[9,10] The major research focus was laid onto realizing highly efficient or white-light-emitting devices. So far, the understanding of the mechanism in CGLs is very limited. Tsutsui and co-workers proposed a model for charge-carrier separation at the interface between Mg-doped tris(8-quinolinolato) aluminum(III) (Alq_3) and V_2O_5 thin films.[6,7] By low-temperature capacitance measurements, they proved a temperature dependence of the described charge-carrier separation and attributed this dependence to thermally activated electron transport via defect states within the V_2O_5 layer. This process leaves a hole carrier within the valence band of the metal oxide, which drifts under the influence of the applied bias toward the cathode.[7] Although other metal oxides were not tested, this model may be applied to other kinds of CGLs consisting of doped organic/metal oxide interfaces. As this model incorporates the presence of a broad distribution of deposition-induced defect states within the metal oxide layer, it may not fit CGLs consisting of doped organic/organic *p-n* junctions. For the latter, Law *et al.* performed ultraviolet photoelectron spectroscopy (UPS) on CGL structures consisting of Mg-doped Alq_3 and tetrafluorotetracyanoquinodimethane (F_4-TCNQ) doped 4,4′,4″-tris(*N*-3-methylphenyl-*N*-phenylamino)-triphenylamine (m-MTDATA) thin films, revealing a large energy shift at the interface due to the presence of a large space-charge density.[10] Furthermore, the authors referred to the model proposed by Tsutsui *et al.*,[7] leaving the mechanism occurring at the interface unclear and subject to further investigation. In this work, a detailed study on organic/organic CGL structures based on F_4-TCNQ doped 4,4′,4″-tris(*N*-1-naphtyl-*N*-phenylamino)-triphenylamine (1-TNATA) and Li-doped 1,3,5-tri(phenyl-2-benzimidazole)-benzene (TPBi) thin films is presented. Energetic shifts at the interface are observed by applying the Kelvin probe (KP) method to doped organic thin films. Furthermore, low-temperature *I-V* measurements have been performed to identify the temperature dependence of the participating physical processes. It will be clearly shown that the process of charge-carrier separation at doped organic/organic interfaces is temperature independent and can be explained by electron tunneling from filled highest occupied molecular orbital (HOMO) states of the hole-transporting layer to unoccupied lowest unoccupied molecular orbital (LUMO) states of the electron-transporting layer through a narrow depletion zone at the interface.

II. EXPERIMENTAL DETAILS

Deposition of the organic thin films and metal contacts were carried out within a 10^{-8} mbar vacuum system with separate deposition chambers for *n* and *p* doping, transport and emitting materials, and metal contacts. The deposition rate for all organic materials was monitored by quartz-crystal monitors and kept constant within the range from 0.02 to 0.1 nm/s. To keep the samples under UHV conditions during the complete deposition and KP characterization cycle, a commercial KP analyzer (McAllistor KPG 6500) was mounted to the vacuum system. The experimental error can be estimated to be lower than 20 meV. A software-controlled Keithley 2400 Source Meter in combination with an Advantest TQ 8221 photodetecting unit was applied for *I-V* and *L-I-V* measurements. Additionally, low-temperature

 ©2007 The American Physical Society

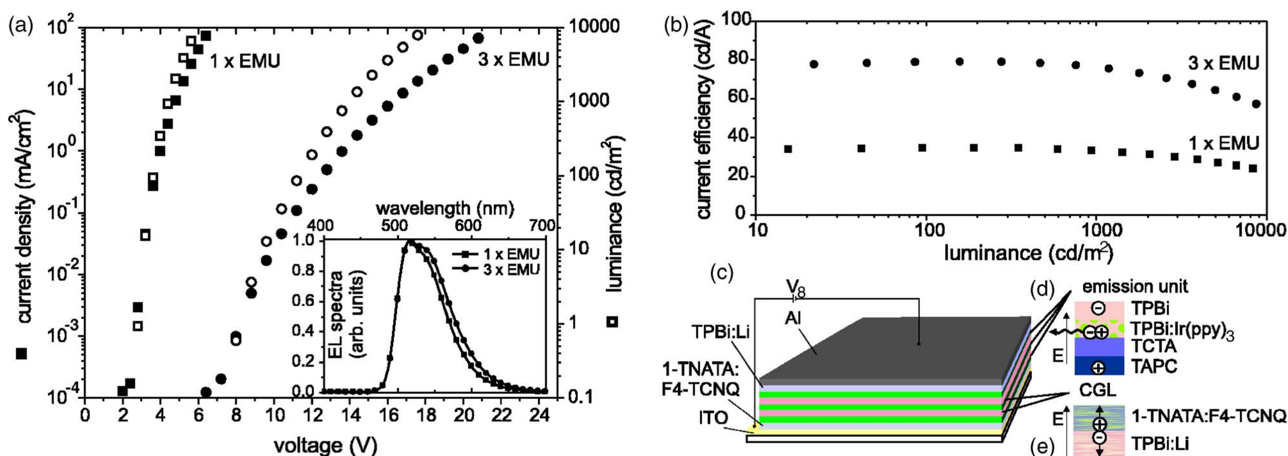

FIG. 1. (Color online) Characteristics and schematic for a stacked OLED. (a) *L-I-V* characteristics for a conventional OLED having one EMU (squares) compared to a stacked OLED with three EMUs (circles). (b) Current efficiency vs luminance for a conventional OLED having one EMU (squares) compared to a stacked OLED with three EMUs. (c) Schematic of a stacked OLED consisting of three EMUs connected by two CGLs. (d) Schematic of a single-emission unit: injected electrons and holes are transported to the recombination zone and recombine to excitons, which decay radiatively. (e) Schematic of a CGL structure: electrons and holes separate upon the application of an external electric field and can be injected into the neighboring EMUs.

I-V measurements down to 40 K were performed by the same setup but within a cryostat. All devices were prepared on commercial indium tin oxide (ITO)-coated glass substrates purchased from Merck. As *p*-type layer, 1-TNATA doped with F_4-TCNQ has been applied. The *n*-type layer consisted of Li-doped TPBi. Doping levels for *p*- and *n*-type doping were optimized by determining the doping concentration for highest conductivity within single-carrier devices. As OLED devices are used for demonstrating the concept of stacking several emission units by CGLs, these emission units (EMUs) consisted of 10 nm of TPBi as hole and exciton blocking layer, fac tris(2-phenylpyridin)iridium ($Ir(ppy)_3$) doped TPBi as the emitting layer, and 10 nm 4,4′,4″-tri(*N*-carbazolyl)-triphenylamin (TCTA) plus 10 nm of 1,1-bis(di-4-tolylaminophenyl) cyclohexane (TAPC) as hole-transporting layers. All devices were completed by a 200-nm-thick Al layer serving as top metal contact (deposition rate: 0.3 nm/s). More detailed information about device structures and layer thickness will be given, if necessary, when these devices are discussed.

III. RESULTS AND DISCUSSION

Figure 1 shows a comparison of a conventional OLED having one EMU and a stacked OLED employing three EMUs connected by organic/organic *p-n* junctions serving as charge generation layers. The device structure of a stacked OLED is depicted schematically in Figs. 1(c)–1(e) It shows that for a given luminance the driving voltage and current efficiency nearly triples, indicating an efficient charge generation at the TPBi:Li/1-TNATA:F_4-TCNQ interface. The improvement factor in current efficiency is slightly smaller than the number of EMUs. As can be derived from the emission spectrum of the two devices, microcavity effects may cause the lower than expected efficiency.[8]

It has to be pointed out that the improvement in current efficiency in our devices can only be explained by additional pairs of charge carriers separated within the CGL unit, as shown in Fig. 1(e). Then electron and hole carriers are injected into the neighboring EMU, where they recombine with the corresponding opposite charge carrier [see Fig. 1(d)]. The latter ones are injected either from another CGL or from the electrodes if the EMU is next to the anode or to the cathode. If no charge carriers were generated at the *p-n* junction, there would be no improvement in the current efficiency, as injected electron-hole pairs can only recombine once. Furthermore, high injection barriers at the organic heterointerfaces and transport barriers resulting from electrons passing mainly hole-transporting layers (HTLs) and holes passing mainly electron-transporting layers (ETLs) would lead to a drastic increase in the driving voltage, as has been observed for a stacked OLED in which no CGL layers were applied.[9] Summarizing our work and the results of other groups published so far, field-assisted charge-carrier generation at doped organic/organic or organic/inorganic interfaces is evident and essential for stacking of OLEDs.[6]

A. Doping profile

Organic/inorganic CGLs consist of a donor-doped electron-transporting layer and a thermally evaporated metal oxide layer. In this case, the field-assisted charge transfer from occupied valence-band states of the metal oxide to LUMO states of the electron-transporting layer was identified as a mechanism for charge separation under reverse bias.[7] Because no significant hole-injection barrier between metal oxide and HTL is present, *p* doping of the HTL was not necessary. For organic/organic interfaces, it has not been evaluated yet if and how different doping schemes at the organic heterojunction affect the efficiency of charge-carrier separation. For this reason, we prepared CGL samples having either a doped *p-n* junction, a partially doped *p-n* junction, or an intrinsic *p-n* junction. In this context, the term *p-n* junction refers to the heterointerface between hole-

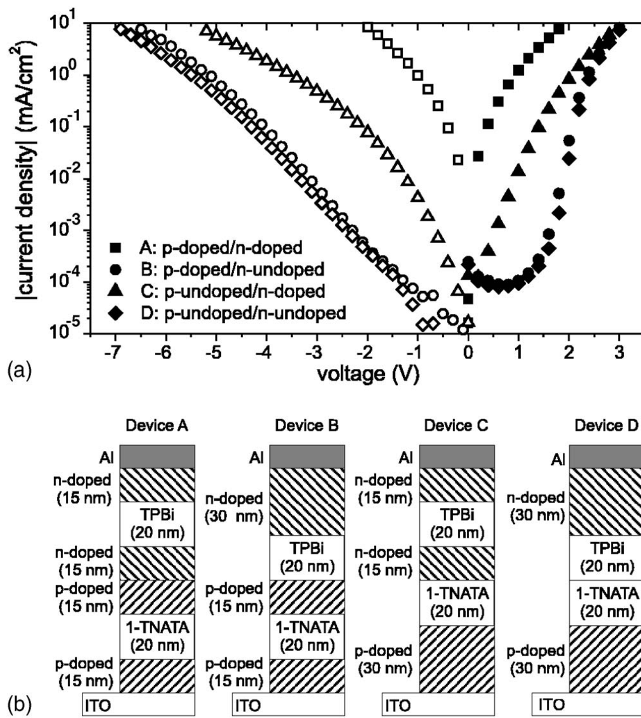

FIG. 2. (a) *I-V* characteristics and schematic for *p*-doped/*n*-doped (squares), *p*-doped/*n*-undoped (circles), *p*-undoped/*n*-doped (triangles), and *p*-undoped/*n*-undoped (diamonds) interfaces. Positive voltage corresponds to ITO electrode biased positively (closed symbols); negative voltage corresponds to Al electrode biased positively (open symbols). (b) Schematic of the devices' layer sequence.

transporting and electron-transporting layers. Detailed information on the device structures and layer thicknesses are given in Fig. 2(b). For all devices, the overall thickness of doped and intrinsic films is kept constant. Figure 2(a) shows the *I-V* characteristics for these devices. Devices B and D show very similar characteristics and display the lowest current densities and a rectification ratio of more than 3 orders of magnitude. In both devices, an intrinsic ETL can be found at the interface. In device C, an intrinsic HTL and a *n*-doped ETL establish the *p-n* junction. Compared to the forward current, a 30 times smaller reverse current is measured, resulting in an asymmetric *I-V* characteristic. Only for device A, which represents doped hole-transporting layer and doped electron-transporting layer adjacent to the *p-n* interface, is a symmetric *I-V* characteristic observed. Under reverse bias (negative voltage), charge injection and recombination or unipolar charge transport can be neglected due to high injection and transport barriers.[6] Therefore, the obtained data suggest that charge generation and extraction into the contacts under reverse bias are as efficient as charge injection and recombination under forward bias.

The symmetry of the *I-V* characteristic of CGL structures can be taken as an indicator for the efficiency of charge generation at the *p-n* interface. As for device C, an asymmetric characteristic is observed and devices B and D exhibit a rectifying behavior; it has to be recorded that for efficient charge generation, both the ETL and the HTL have to be doped (device A).

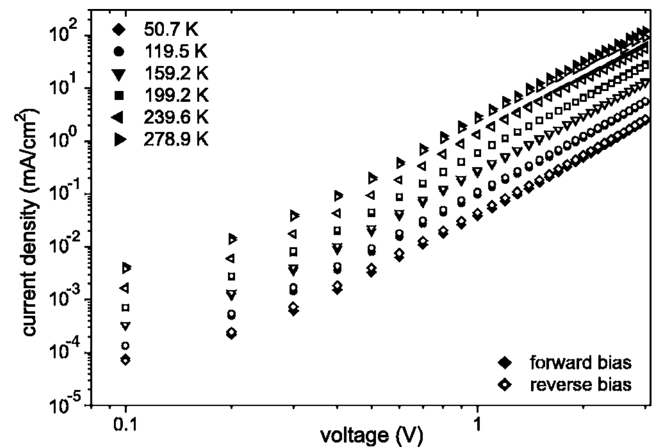

FIG. 3. Temperature-dependent *I-V* characteristics of a CGL structure. Forward bias corresponds to positive voltage applied to the ITO electrode (closed symbols); reverse bias corresponds to positive voltage applied to the Al electrode (open symbols).

B. Low temperatures

For further investigations on the thermal dependence of the CGL architecture proposed in this work, we prepared simple CGL samples comprising of a F_4-TCNQ doped 1-TNATA film and a Li-doped TPBi layer, both 50 nm in thickness, deposited onto an ITO substrate and capped with 100 nm of Al as top electrode. Temperature-dependent *I-V* characteristics of this device are shown in Fig. 3.

Upon applying a positive voltage to the ITO electrode, charge carriers are injected at both electrodes and transported to the *p-n* interface where they recombine. A common model for charge injection from metallic contacts into *n*- or *p*-doped organic semiconductors describes tunneling of charge carriers through a narrow space-charge region at the interface.[11,12] Unlike the Richardson-Schottky model, which gives a good approximation for charge injection into intrinsic organic semiconductors[11] and assumes thermally activated hopping over the injection barrier, no explicit temperature dependence is expected for the Fowler-Nordheim (FN) tunnel mechanism. We assume that the recombination of electrons and holes at the interface is independent of temperature within the observed temperature range. Due to the structural disorder of the organic thin films and only weak intermolecular coupling, the charge-carrier transport in organic solids is often described as thermally activated hopping of localized charge carriers. The temperature dependence of the forward characteristic is attributed to a lower carrier mobility for lower temperatures.

Under reverse bias, the device shows the same current density for a given temperature and voltage, leading to symmetric *I-V* characteristics for all temperatures within the given range. Considering that the temperature dependence of the hopping mobility will affect the reverse current in the same way as it affects the forward current and that the symmetry in the *I-V* characteristics is maintained for all temperatures, the charge-carrier separation must be independent of temperature. Therefore, a temperature dependence of the charge separating mechanism as reported for organic/

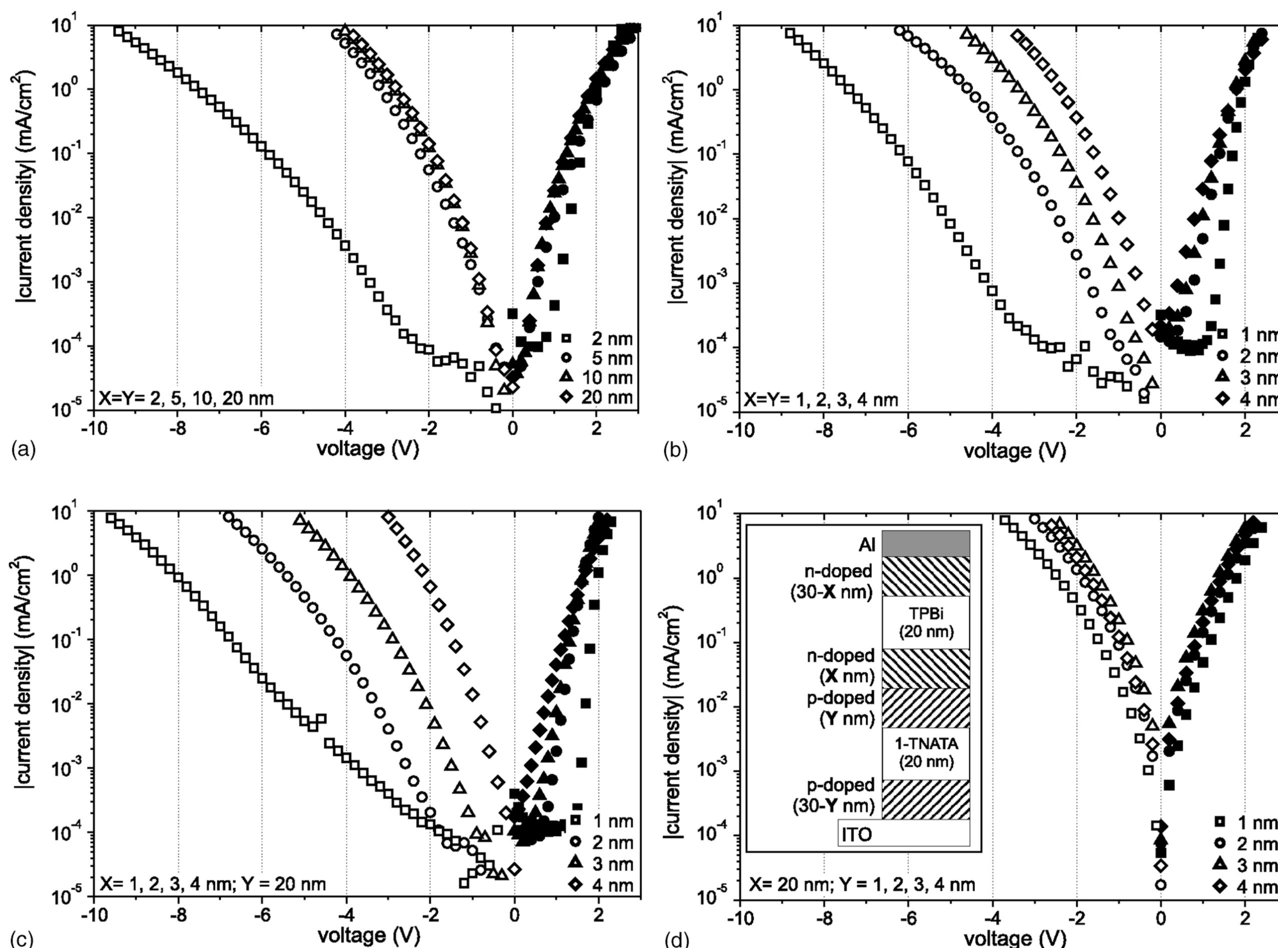

FIG. 4. *I-V* characteristics for CGL samples with different thicknesses of the *p*- and *n*-doped layers adjacent to the *p-n* interface. Positive voltage corresponds to ITO electrode at positive bias (closed symbols); negative voltage corresponds to Al electrode at positive bias (open symbols). (a) Thickness of *p*- and *n*-doped layers varied between 2 and 20 nm. (b) Thickness of *p*- and *n*-doped layers varied between 1 and 4 nm. (c) Thickness of *p*-doped layer kept constant at 20 nm; thickness of *n*-doped layer varied between 1 and 4 nm. (d) Thickness of *p*-doped layer varied between 1 and 4 nm; *n*-doped layer was kept constant at 20 nm. The inset displays a schematic of the device structure for all sets of devices.

inorganic CGL architectures[7] was not observed for organic/organic CGLs. Thus a field-only driven mechanism is most likely.

C. Thickness dependence

The dependence of the electrical properties of CGL structures on the thickness of the doped regimes adjacent to the *p-n* heterojunction will be discussed next. For this reason, CGL samples with different thicknesses of the doped layers have been prepared. As displayed in the inset of Fig. 4(d), the thickness of the doped layers adjacent to the *p-n* interface can be adjusted by shifting the position of an undoped ETL (TPBi) or HTL (1-TNATA) without changing the ratio of the doped layers' thickness compared to the total device thickness. This means that a change in the characteristics cannot be attributed to a change in the ratio of the thickness of doped and intrinsic layers. For charge injection, at least 10-nm-thick electron-injection layer and hole-injection layer have been employed next to the cathode or anode, respectively. For simplicity, the thickness of the *n*-doped layer next to the interface will be denoted as X and the thickness of the *p*-doped layer will be short-termed as Y [inset of Fig. 4(d)]. Figure 4 shows the *I-V* characteristics for four different sets of CGL samples.

For Fig. 4(a), X and Y are equal and altered from 2 nm to 20 nm. Only the device with 2 nm *n*- and *p*-doped layers exhibits a significant difference in the *I-V* characteristic. Under forward bias, only a slight increase of driving voltage for low current densities can be observed, but reversing the bias leads to a large increase in driving voltage for the $X=Y=2$ nm device. For a more detailed view, the experiment was repeated, again keeping X and Y equal, now ranging from 1 to 4 nm with 1 nm stepsize. The *I-V* characteristics for this set of samples are displayed in Fig. 4(b). As for these extremely thin layers, the run-to-run reproducibility becomes an issue; the values from Figs. 4(a) and 4(b) cannot be compared quantitatively and have to be discussed separately and under qualitative aspects. Again, under forward bias, only a small increase in driving voltage with decreasing thickness of the doped layers is observed. For reverse bias, the driving voltage for a given current density gradually in-

creases for decreasing thickness of the doped layers. This leads to a strong asymmetry of the *I-V* characteristics, indicating a less efficient charge generation for devices with less than 5-nm-thick *p*- and *n*-doped layers. As the results discussed in Fig. 2 suggest that the symmetry of the *I-V* characteristics is affected predominantly by doping of the *n*-doped layer, it has to be checked if this is reflected when the thickness of the doped layers are changed separately. Figure 4(c) shows the *I-V* characteristics of CGL samples for which X varied within the range from 1 to 4 nm and Y was kept constant at 20 nm. The characteristics seem to be very similar to those of Figs. 4(b), with an increasing asymmetry for decreasing thickness of the *n*-doped layer. When X is kept constant and Y is varied between 1 and 4 nm, a very different image is revealed, as shown in Fig. 4(d). For all devices, the *I-V* characteristics are nearly symmetric and exhibit slightly increasing driving voltages under reverse bias with decreasing thickness of the *p*-doped layer. Compared to the asymmetry in Figs. 4(b) and 4(c), and the increase in driving voltage and the asymmetry can be neglected. It has to be noted that no closed films can be expected for only 1 nm layer thickness. The increase of driving voltage in the positive regime for the 1-nm-thin *p*-doped layer may be an indicator of this. As for thicker layers, no remarkable difference in the forward characteristics is observed; we expect closed films for thicknesses greater than 1 nm. Summarizing the results shown in Fig. 4, it is evident that a minimum thickness of 5 nm for the *n*- and *p*-doped layers next to the interface is necessary for efficient charge generation. Further, the charge generation seems to be more sensitive to the thickness of the *n*-doped layer.

D. Kelvin probe measurements

To gain a deeper understanding of the dominating mechanism leading to charge generation at organic/organic heterointerfaces, we measured the energy-level alignment at the interface by using a KP analyzer. Figure 5 shows the evaluation of the work function ϕ at different positions within the device. As the KP technique does not provide depth resolution but rather delivers the surface work function, we incrementally deposited the CGL stack and measured the corresponding work function after each deposition step. Close to the interfaces, an increment size of 1 nm is useful and several 10 nm steps are sufficient at a certain distance from the interface for resolving the energy-level alignment.

We measured the work function of an undoped HTL/ETL stack [see Fig. 5(a)] and for the so far described CGL stack [see Fig. 5(b)] deposited onto differently conditioned substrates. As the work function of the reference tip is not given by the manufacturer, we referenced the measurements to the substrate's surface work function. Literature values for ITO vary from 4.1 to 5.2 eV depending on the pretreatment of the substrate and the measurement technique.[13–18] A work function of 4.5 eV for as-received ITO substrates complies with most of the publications.[13–15] Furthermore, it is documented that an oxygen plasma treatment prior to the deposition of organic materials leads to an increase of work function of about 0.5 eV.[14,16,18] Therefore we assume a work function of

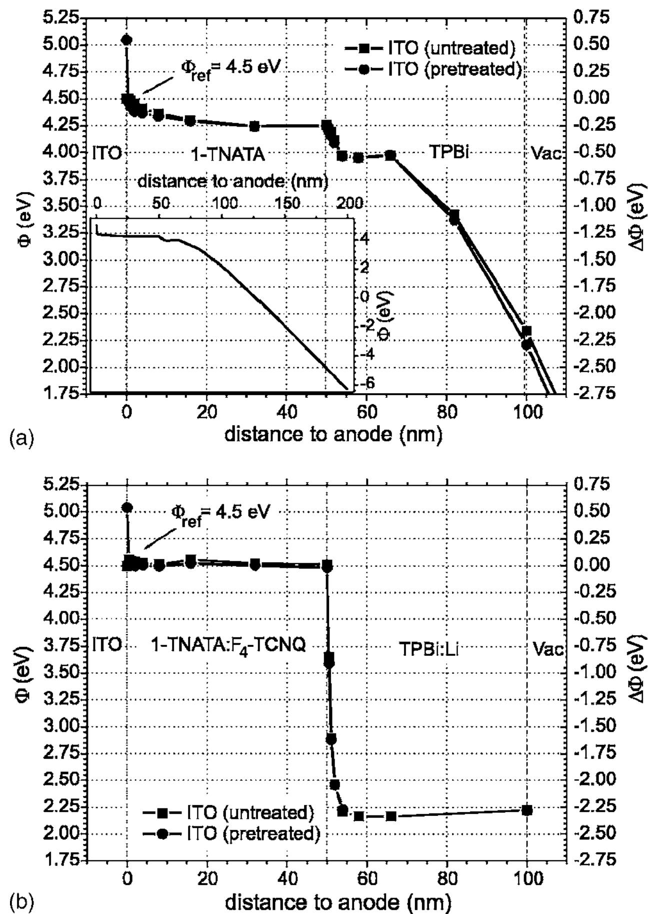

FIG. 5. Work function obtained from KP measurements as a function of the film thickness, relative to the ITO substrate's work function for (a) an undoped *p-n* heterojunction (inset: progression of the work function for a thicker TPBi film) and (b) a doped *p-n* heterojunction.

4.5 eV for untreated ITO and 5.0 eV for ITO films exposed to an oxygen plasma prior to the organic layer deposition. For both types of samples (undoped and doped), a good match of the energy levels can be observed for both substrates, indicating that the energy-level alignment is independent of the pretreatment of the substrate. For the undoped device, a slight downward shift of the work function of 0.15 eV is observed with increasing 1-TNATA thickness. Upon the deposition of undoped TPBi, the work function decreases within the first 3 nm to about 0.3 eV above the value for undoped 1-TNATA and is constant until 15 nm of TPBi are deposited. The vacuum-level shift at the interface can be attributed to a small interfacial dipole as has been observed for other undoped organic/organic interfaces.[19] For thicker undoped TPBi layers, the work function shows a steep linear decrease of several eV. This effect has been investigated by Ito *et al.* in 2002.[20] They observed a spontaneous buildup of surface potential upon deposition of Alq_3 onto a Au substrate. The surface potential determined by the KP method reached 26 V for a 560-nm-thick film and was explained by a model in which a preferential orientation of the dipole moments of Alq_3 leads to the observed surface potential. Furthermore, it has been demonstrated that irradiating

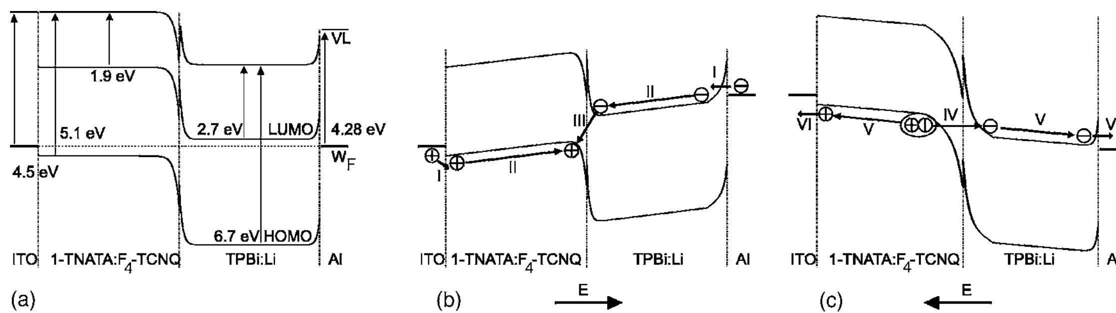

FIG. 6. Energy-level alignment for a CGL device: (a) no external bias, (b) under forward bias (recombination), and (c) under reverse bias (charge generation).

the sample with visible light ($\lambda < 600$ nm) removes the surface potential. This has been attributed to the loss of preferential orientation upon electronic excitation of the molecules. We measured a change of surface potential of about 10.3 eV upon deposition of 135 nm of TPBi, as shown in the inset of Fig. 5(a). The slope of the rise in surface potential is about 0.07 eV/nm and is close to the value determined by Ito *et al.* for Alq_3 (0.05 eV/nm). For this reason, we expect that a similar mechanism holds for the observed spontaneous buildup of surface potential in undoped TPBi films. In addition, we expect that the preferential orientation will also be removed by charges injected into the film upon applying an external bias. Therefore, the characteristics of undoped devices should not be affected by the measured phenomenon, which will be neglected in the further discussion. Overall, only a small interfacial dipole can be observed between 1-TNATA and TPBi. The energy-level alignment at the interface significantly changes when doped ETLs and HTLs are investigated.

Figure 5(b) shows the progression of the work function with film thickness for doped transport layers. Upon deposition of 1-TNATA doped with F_4-TCNQ onto the substrate, the work function is measured to be 4.5 eV and independent of film thickness and substrate pretreatment. As this value equals the work function assumed for untreated ITO as reference substrate, no interfacial dipole should be expected in this case. For the oxygen-plasma-treated ITO, an interfacial energy shift of 0.5 eV can be observed, which corresponds to the difference in work functions. At the *p*-*n* junction between the HTL and the Li-doped TPBi ETL, the energy level drastically shifts toward lower values. Within the first nanometer, the work function changes by 1.6 eV. As the prior results suggested that 1 nm of deposited film is needed for a closed surface, this shift in work function is most likely due to an interfacial dipole. The value of the work function further decreases until the curve saturates for film thicknesses above 5 nm at a work function about 2.3 eV lower than that measured for the *p*-doped HTL. The observed band bending is an indicator of the exchange of free charge carriers at the *p*-*n* junction leading to a space-charge region of about 5 nm thickness.

In a recent paper, Law *et al.* showed results for UPS measurements on a CGL structure very similar to the one employed in our work. The reported structure consisted of Mg-doped Alq_3 as *n*-type electron-transporting layer and m-MTDATA doped with F_4-TCNQ as *p*-doped hole-transporting layer.[10] They observed an interfacial dipole of 0.46 eV and an upward band bending of 1.36 eV, giving a total energy shift of 1.82 eV. Due to the fact that KP measurements do not allow to clearly separate the influence of interfacial dipoles from the influence of space charges, only the overall energy shifts should be compared. The shift of work function of about 2.3 eV within Li-doped TPBi is close to the vacuum-level shift of 1.82 eV within m-MTDATA doped with F_4-TCNQ measured by UPS. Furthermore, the width of the space-charge region within the ETL was determined to be about 5 nm, which complies very well to the value (6.4 nm) given in the mentioned publication.[10] As both techniques—UPS and KP—are surface sensitive, we assume that the deposition of the *n*-doped TPBi ETL on top of the *p*-doped 1-TNATA HTL also leads to a thin space-charge region within the HTL.

E. Energy-level alignment

The presented results lead to the conclusion that at doped organic *p*-*n* junctions the exchange of charge carriers leads to an upward band bending, which is on the same order of magnitude as the optical band gap leading to a thin depletion zone within both layers adjacent to the heterointerface. Figure 6 depicts the energy-level alignment and compares the involved physical processes for forward and reverse bias, taking a simple CGL-diode structure as example. The given values for the work function of the electrodes[13,21] and the HOMO and LUMO levels of the organic materials[22,23] are taken from literature. According to the presented KP measurements, the Fermi level within the *p*-doped HTL lies 4.5 eV below the vacuum level (VL) and 0.6 eV above the HOMO level. Considering literature values for Cs-doped CuPc films,[24] the position of the Fermi level within the *n*-doped ETL has been assumed to be 0.2 eV lower than the LUMO edge. At the *p*-*n* interface, the exchange of free charge carriers and a possible interface dipole have to be taken into account. The downward band bending in the ETL quantitatively corresponds in value and width to the results obtained by KP. The upward band bending was approximated in energy and width by the values given by Law *et al.*[10] Both upward band bending within the HTL and downward band bending in the ETL as well as an interfacial dipole ($\Delta E = 1$ eV) have been included in the vacuum-level alignment shown in Fig. 6(a). When no external bias is applied, equilibrium conditions demand for a common Fermi level

throughout the device [see Fig. 6(a)]. The energy-level alignment is not expected to be completely correct in quantitative values, but it qualitatively suffices to explain the observed charge generation. For the reason of simple understanding, the VL and explicit values for energy levels are not included in Figs. 6(b) and 6(c).

Under forward bias, holes are injected from the anode into the HTL and electrons are injected from the cathode into the ETL. In Fig. 6(b), the charge injection is denoted as I at both electrodes. For highly doped organic semiconductors, it has been demonstrated that at the interface toward the electrode, band bending and charge injection via FN tunneling through a narrow space-charge region may occur,[25] as shown for the electron injection from the cathode. At the anode, flatband conditions apply and holes have to pass a small injection barrier of 0.35 eV. The injected holes are transported—most likely via hopping—toward the heterointerface (II). The tilted energy levels within the bulk of the HTL and ETL account for the voltage drop across the transport layers due to the limited bulk conductivity of the organic materials. At the heterointerface, electrons and holes recombine. The recombination mechanism shall not be discussed in detail, but recombination via gap states, dopant states, or excited complexes at the interface may occur (III). In all cases of recombination, accumulation of both carrier types close to the heterointerface is expected, resulting in a significant voltage drop across the interface. For higher external fields, LUMO level alignment is expected, leading to a direct injection of electrons into the HTL. Then, most of the excitons formed within the HTL are quenched by the high acceptor concentration and only negligible light emission has been observed (not shown here).

In the case of reverse bias, it has already been demonstrated that only charge generation at the *p*-*n* interface can lead to a significant current. Under zero bias, the LUMO level of the ETL lies only about 300 meV above the HOMO level of the electron-transporting layer.[10] Applying a reverse bias even lowers the position of the ETL's LUMO level with respect to the HOMO level of the HTL, which are separated by a few-nanometer-thick energy barrier. There is a finite probability σ_{pn} that electrons may tunnel through this barrier from occupied HOMO states of the HTL to unoccupied LUMO states of the ETL (IV). The probability σ_{np} for the reverse process IV^{-1} of electrons tunneling from filled LUMO states in the ETL to unfilled HOMO states in the HTL equals σ_{pn}, but the process can be neglected, as almost no free charge carriers are present close to the *p*-*n* interface due to the depletion of the space-charge region. Furthermore, electrons tunneling from the HOMO of the HTL into the LUMO of the ETL will immediately be driven away from the interface by the external electric field (V). This leaves a hole in the HOMO of the HTL, which in the same way immediately escapes the space-charge region at the interface (V). As in the regarded case no or only small energy barriers are present at the electrodes, the charge carriers can easily escape (VI). Considering the case of a stacked OLED, these charge carriers can be injected into neighboring recombination zones where they recombine with charge carriers injected from the electrodes of the stacked OLED.

As tunneling processes, in general, are regarded as temperature independent, the model, which is developed from the experimental data collected via KP measurements and thickness-dependent *I*-*V* characteristics, fits well to the results for low-temperature *I*-*V* characteristics.

IV. SUMMARY

In summary, we demonstrated that in stacked OLEDs doped organic *p*-*n* heterojunctions act as interconnecting units between two or more recombination and emission units by separating charges under the influence of a reverse bias. It was shown that both HTL and ETL adjacent to the heterointerface have to be doped for efficient charge generation. From low-temperature *I*-*V* characteristics, it has been derived that no explicit temperature dependence applies for the charge generating process. Further investigations by thickness-dependent *I*-*V* characteristics and KP measurements demonstrated a large band bending at the interface and a depletion zone within the ETL of about 5 nm thickness. An appropriate model for the charge generation was presented as direct tunneling from occupied HOMO states within the HTL to unoccupied LUMO states within the ETL.

ACKNOWLEDGMENT

The authors would like to thank the German Federal Ministry of Education and Research (BMBF) for funding part of this work under Contract No. FKZ 13N8995 (OPAL).

*Email address: michael.kroeger@ihf.tu-bs.de
†Corresponding author. Email address: h2.johannes@ihf.tu-bs.de

[1] G. Gu, G. Parthasarathy, P. E. Burrows, P. Tian, I. G. Hill, A. Kahn, and S. R. Forrest, J. Appl. Phys. **86**, 4067 (1999).
[2] H. Kanno, N. C. Giebink, Y. Sun, and S. R. Forrest, Appl. Phys. Lett. **89**, 023502 (2006).
[3] C.-C. Chang, J.-F. Chen, S.-W. Hwang, and C. H. Chen, Appl. Phys. Lett. **87**, 253501 (2005).
[4] F. Guo and D. Ma, Appl. Phys. Lett. **87**, 173510 (2005).
[5] C.-W. Chen, Y.-J. Lu, C.-C. Wu, E. H.-E. Wu, C.-W. Chu, and Y. Yang, Appl. Phys. Lett. **87**, 241121 (2005).
[6] T. Tsutsui and M. Terai, Appl. Phys. Lett. **84**, 440 (2004).
[7] M. Terai, K. Fujita, and T. Tsutsui, Jpn. J. Appl. Phys., Part 2 **44**, L1059 (2005).
[8] T.-Y. Cho, C.-L. Lin, and C.-C. Wu, Appl. Phys. Lett. **88**, 111106 (2006).
[9] L. S. Liao, K. P. Klubek, and C. W. Tang, Appl. Phys. Lett. **84**, 167 (2004).
[10] C. W. Law, K. M. Lau, M. K. Fung, M. Y. Chan, F. L. Wong, C. S. Lee, and S. T. Lee, Appl. Phys. Lett. **89**, 133511 (2006).
[11] W. Gao and A. Kahn, Org. Electron. **3**, 53 (2002).
[12] W. Gao and A. Kahn, J. Appl. Phys. **94**, 359 (2003).
[13] Y. Park, V. Choong, Y. Gao, B. R. Hsieh, and C. W. Tang, Appl. Phys. Lett. **68**, 2699 (1996).

[14] K. Sugiyama, H. Ishii, Y. Ouchi, and K. Seki, J. Appl. Phys. **87**, 295 (2000).
[15] X. M. Ding, L. M. Hung, L. F. Cheng, Z. B. Deng, X. Y. Hou, C. S. Lee, and S. T. Lee, Appl. Phys. Lett. **76**, 2704 (2000).
[16] D. J. Milliron, I. G. Hill, C. Shen, A. Kahn, and J. Schwartz, J. Appl. Phys. **87**, 572 (2000).
[17] H. Y. Yu, X. D. Feng, D. Grozea, Z. H. Lu, R. N. S. Sodhi, A.-M. Hor, and H. Aziz, Appl. Phys. Lett. **78**, 2595 (2001).
[18] M. G. Mason, L. S. Hung, C. W. Tang, S. T. Lee, K. W. Wong, and M. Wang, J. Appl. Phys. **86**, 1688 (1998).
[19] A. Kahn, W. Zhao, W. Gao, H. Vasquez, and F. Flores, Chem. Phys. **325**, 129 (2006).
[20] E. Ito, Y. Wahizu, N. Hayashi, H. Ishii, N. Matsuie, K. Tsuboi, Y. Ouchi, Y. Harima, K. Yamashita, and K. Seki, J. Appl. Phys. **92**, 7306 (2002).
[21] D. R. Lide, *Handbook of Chemistry and Physics* (CRC, Boca Raton, FL, 2000).
[22] S.-C. Lo, N. A. H. Male, J. P. J. Markham, S. W. Magennis, P. L. Burn, O. V. Salata, and I. D. W. Samuel, Adv. Mater. (Weinheim, Ger.) **14**, 975 (2002).
[23] A. Böhler, *Organische Elektrolumineszenzdisplays* (Shaker, Aachen, 1999).
[24] L. Yan, N. J. Watkins, S. Zorba, Y. Gao, and C. W. Tang, Appl. Phys. Lett. **79**, 4148 (2001).
[25] W. Gao and A. Kahn, Appl. Phys. Lett. **79**, 4040 (2001).